10-20-2018

Strain Monitoring of Concrete Components Using Embedded Carbon Nanofibers/Epoxy Sensors

Yanlei Wang

Yongshuai Wang

Baoguo Han

Baolin Wan

Gaochuang Cai

See next page for additional authors

Authors

Yanlei Wang, Yongshuai Wang, Baoguo Han, Baolin Wan, Gaochuang Cai, and Zhizheng Li

Strain Monitoring of Concrete Components Using Embedded Carbon Nanofibers/Epoxy Sensors

Yanlei Wang
State Key Laboratory of Coastal and Offshore Engineering, School of Civil Engineering, Dalian University of Technology, Dalian, Liaoning 116024, China
Yongshuai Wang
State Key Laboratory of Coastal and Offshore Engineering, School of Civil Engineering, Dalian University of Technology, Dalian, Liaoning 116024, China
Baoguo Han
State Key Laboratory of Coastal and Offshore Engineering, School of Civil Engineering, Dalian University of Technology, Dalian, Liaoning 116024, China
Baolin Wan
Department of Civil, Construction and Environmental Engineering, Marquette University, Milwaukee, WI
Gaochuang Cai

Laboratory of Solid Structures, University of Luxembourg, Luxembourg L1359, Luxembourg

Zhizheng Li

State Key Laboratory of Coastal and Offshore Engineering, School of Civil Engineering, Dalian University of Technology, Dalian, Liaoning 116024, China

Highlights

- Embedding CNFs/epoxy sensors into concrete components is studied at first time.
- The piezoresistive performances of the CNFs/epoxy sensors are evaluated.
- A compensation circuit is proposed to eliminate the effect of temperature.
- The calibration and monitoring curves exhibited a consistent variation trend.

Abstract

In this study, embedded strain sensors based on the principle of piezoresistivity were fabricated by epoxy-based composites filled with different contents of carbon nanofibers (CNFs). The piezoresistive performances and relevant parameters including gauge factor, linearity, repeatability and hysteresis of these sensors were investigated. A compensation circuit was proposed to eliminate the influence of temperature on sensing signals of the sensors. The CNFs/epoxy sensors were embedded into concrete cylinders to monitor their compressive strains under monotonic and cyclic loadings, thereby assessing practical applications of the CNFs/epoxy sensors as strain sensors for monitoring concrete structures. The results indicate that the sensors containing 0.58 vol% of CNFs, which have a gauge factor of 37.1, a linearity of 5.5%, a repeatability of 3.8% and a hysteresis of 6.3%, exhibited better piezoresistive performance compared to those containing 0.29 vol% of CNFs. The calibration and monitoring curves exhibited a consistent variation trend when the cylinders embedded with sensors were subjected to monotonic and cyclic loadings. This demonstrates that the CNFs/epoxy sensors have considerable potential to be used as embedded strain sensors for structural health monitoring of concrete structures.

Keywords

Carbon nanofibers (CNFs), Embedded sensor, Strain monitoring, Concrete cylinders, Piezoresistivity

1. Introduction

Civil infrastructures often suffer deterioration, damage accumulation or even sudden collapse due to fatigue load, environmental factors and a range of natural disasters, etc. Structural health monitoring (SHM) is a method to continuously monitor and evaluate the state of civil infrastructures. SHM systems use a group of sensors to measure real-time data of strain, displacement, temperature, etc. of structures, which help engineers and owners to detect anomalies in the structure's performance in timely manner [1]. With the aid of SHM, the structural strengthening or retrofitting measures can be timely established to ensure the safety and serviceability of the structure [2].

Conventional strain sensors, such as electrical resistance strain gauges, fiber optic sensors and piezoelectric ceramics, have been widely used in SHM [3], [4]. However, utilization of these sensors is often limited due to some drawbacks including low sensitivity, high cost, poor durability, and fragility. In these circumstances, using piezoresistive composites to fabricate strain sensors has attracted extensive attention [2]. The sensors prepared by piezoresistive composites have advantages of multi-functionality, high sensitivity, cost effectiveness, excellent durability, and relatively easy fabrication processes, which are distinct from the conventional SHM sensors [5], [6]. The theory making these sensors work is the principle of piezoresistivity,

which is defined as a change in electrical resistance in response to the mechanical strain applied to the composites [7]. One common technique of the piezoresistive sensors are to incorporate electrically conductive reinforcement fillers (e.g., carbon nanotubes (CNTs) [2], [8], [9], carbon nanofibers (CNFs) [10], [11], [12], [13], graphene nanoplatelets [14], carbon black [9], [15], and nickel powder [16]) into dielectric or semiconducting matrix (e.g., rubber [17], epoxy [10], [18], and cement [19], [20], [21], [22], [23]).

Considerable number of researches have proved that it is feasible to prepare the sensors by piezoresistive composites for strain monitoring [18], [24], [25], [26], [27], [28]. Monteiro et al. [27] investigated a piezoresistive carbon black cement composite for traffic monitoring. A linear and reversible piezoresistive performance was found with gauge factors ranging from 40 to 60. Nam et al. [28] investigated the piezoresistive sensing capabilities of glass and carbon fiber-reinforced plastic composites incorporating CNTs and concluded that these composites showed continuous sensing characteristics. Luo et al. [25] explored the piezoresistive properties of cement composites reinforced by functionalized CNTs. Experimental results indicated that excellent piezoresistive properties were achieved at the doping level of 0.3% by weight, wherein high strain sensitivity was recorded as 286.6 for the cases of adding small amounts of surfactant.

Most current researches [18], [24], [25], [26], [27], [28] mainly focus on the piezoresistive performances of the sensors themselves under different conditions. However, only a few researches studied the strain sensing capability of piezoresistive sensors embedded into concrete structures have been undertaken [29], [30], [31], [32]. Xiao et al. [30], [31] investigated strain sensing properties of cement-based sensors embedded into concrete cylinders and beams, respectively. The results indicated that the embedded cement-based sensors had nice strain-sensing abilities. However, cement-based sensors are greatly affected by environmental humidity. Therefore, humidity insulation method should be used to guarantee the sensing precision of cement-based composites under various ambient conditions [30]. Additionally, the polarization effect of cement matrix adversely affects the accuracy of the monitoring [33]. Compared to cement, epoxy has excellent chemical resistance, wear resistance, electric insulation, waterproof function and large deformation range. If it was used as the matrix for the compressive strain sensors, it could not only eliminate the effects of humidity and polarization, but also enable the whole process monitoring of steel or fiber reinforced polymer (FRP) confined concrete structures with a large ultimate failure strain subjected to compressive loadings, which cannot be achieved by the cement-based sensors with a relative small strain monitoring capacity. Therefore, it is worth to study the performance of embedded epoxy-based sensors for strain monitoring of concrete components subjected to compression.

In this study, the sensors were prepared by CNFs/epoxy composites containing two different contents of CNFs. The piezoresistive performances of the strain sensors themselves were investigated firstly, followed by the exploration of relevant parameters including gauge factor, linearity, repeatability and hysteresis. Secondly, a compensation circuit was proposed to eliminate the influence of temperature on sensing signals of the sensor. Finally, concrete cylinders embedded with CNFs/epoxy sensors were subjected to monotonic and cyclic loadings to explore the strain sensing capability of the sensors, thereby assessing practical applications of the CNFs/epoxy sensors as compressive strain sensors for concrete structures.

2. Experimental program

2.1. Materials

Pyrograf-III PR-24-XT-HHT (manufactured by Prograf Products, Inc., USA), which are heat treated CNFs with diameters of 70–200 nm and lengths of 50–200 μm, were employed as the nanofillers. The properties of the CNFs provided by the manufacturer are shown in Table 1. The epoxy used as the matrix of

the nanocomposite was produced by Tianjin Swancor Wind Power Materials Co., Ltd., China. The epoxy is mixed by two parts: SWANCOR 2511-1A (main agent) and SWANCOR 2511-1BS (curing agent) with a ratio of 10:3 in weight, or 30:11 in volume. It has low viscosity, moderate gel time, nice mechanical properties, high heat deflection temperature (HDT), and good wettability to carbon fibers. The CNFs in the amount of 0.29% and 0.58% by volume of composite were added to the composites, and the corresponding sensors are called $S_{0.29}$ and $S_{0.58}$, respectively, in this paper. Acetone was used as diluting agent in the amount of 2% by volume of composite. Copper wire mesh with the size of 20 mm × 30 mm was used as the electrodes of the sensors. Commercial ready mixed concrete was used for the construction of the concrete cylinders. The mean 28-day compressive strength of the concrete cylinders was 33.5 MPa.

Table 1. Properties of the CNFs.

Diameter (nm)	Length (μm)	Aspect ratio	Surface area (m^2/gm)	Moisture (wt%)
70–200	50–200	250–2800	41	<5

2.2. Specimens

2.2.1. CNFs/epoxy sensors

It is well established that the homogeneity of nanofibers dispersion into the epoxy matrix is one of the most important factors affecting the composite's electrical and piezoresistive performance. Two methods, including mechanical stirring and ultrasonic treatment, were used to disperse CNFs into epoxy matrix in this research. The CNFs/epoxy sensors were prepared by following procedure as shown in Fig. 1: (1) Different amounts of CNFs (0.29 vol% and 0.58 vol%) were dispersed into acetone by a mechanical stirrer (Model SFJ-400, Shanghai Modern Environmental Engineering Technology Co., Ltd., China) at high speed (1500 r/min) for 10 min, and then sonicated by Branson 2800 Ultrasonic Cleaner (Model 2510 E-DTH, 100 W 40 kHz, Branson Ultrasonic Co., Ltd., USA) for 8 h at 20 °C to get CNFs-acetone mixture. (2) Heated (at 60 °C for 2 min) SWANCOR 2511-1A was dissolved in the CNFs-acetone mixture via stirring at high speed (1500 r/min) for 20 min and ultrasonically dispersing at 60 °C for 8 h to get a slurry-like mixture. (3) The mixture was placed in a vacuum oven (Model DZ-2BC, Tianjin Taisite Instrument Co., Ltd., China) to remove acetone and air bubbles. (4) After the mixture was cooled, the curing agent (SWANCOR 2511-1BS) was added and mixed by mechanical stirring at low speed (500 r/min) for 5 min. (5) The CNFs/epoxy mixture was poured into a silicone mold, which was brushed a layer of oil for easily removing the specimen after curing, and two copper wire mesh electrodes were embedded in the mixture. On one hand, the size of the sensor needs to be as small as possible in order to prevent the sensor from damaging the concrete structure. On the other hand, it is difficult to place the sensor in concrete cylinder if it is too small. According to the research of Han et al. [16], the size of the sensor was set to 20 mm × 20 mm × 40 mm. (6) The sensors were pre-cured at room temperature for 24 h followed by a post-cure for additional 8 h at 80 °C.

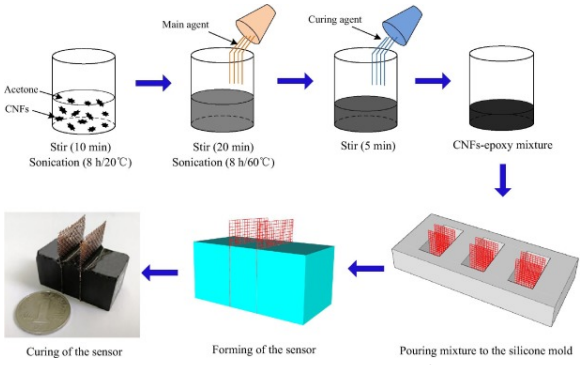

Fig. 1. Preparation process of the CNFs/epoxy sensors.

2.2.2. Concrete cylinders

The concrete cylinders with 150 mm in diameter and 300 mm in height were prepared by following procedure: (1) The calibrated sensor was placed at the center of a polyvinyl chloride (PVC) mold. The sensor was tied to a thin steel wire that had been fixed to the PVC mold. (2) Concrete was slowly poured into the PVC mold. (3) An external vibrator was used to compact concrete after pouring. (4) The cylinders were demolded after 24 h and then cured in a curing room maintaining temperature of 20 ± 3 °C and relative humidity of 95% for 28 days.

2.3. Measurements

2.3.1. Piezoresistive test for sensors

The piezoresistive experiments were performed by applying monotonic and cyclic uniaxial loadings, and simultaneously measuring the strain and the electrical resistance of the CNFs/epoxy sensors. The load was applied by an electronic universal testing machine (Model WDE-200E, Jinan Gold Testing Machines Inc., China) under displacement control. Two cyclic loading paths were applied in this research. Loading type 1 (shown in Fig. 2a) consisted of eight load-unload cycles with constant amplitudes of 25 MPa. Loading type 2 (shown in Fig. 2b) consisted of five cycles with incremental amplitudes of 10, 15, 20, 25 and 35 MPa, and repeated three times for each amplitude. In this study, six specimens of $S_{0.29}$ and $S_{0.58}$ CNFs/epoxy sensor were used for piezoresistive test. For each type of sensors, three specimens were tested under monotonic uniaxial loads until their failures, and the remaining three specimens were first subjected to constant amplitude cyclic loading and then subjected to incremental cyclic loading to simulate realistic loading conditions. The two-electrode method was chosen to measure the electrical resistance rather than the four-electrode method due to its better suitability in terms of implementation [27]. During the test process, the DC resistance was tested by two-electrode method via the Keithley 2100 digital multimeter (Keithley Instruments Inc., USA) and the strain was monitored by one pair of electrical resistance strain gauges which were glued symmetrically in the axial direction at the opposite sides of the middle section of the sensor sample. The DH3820 strain acquisition device (Donghua Testing Technology Co., Ltd., China) was employed to record strain data. The experimental setup of piezoresistive test is shown in Fig. 3. In order to explore the effect of loading rate on piezoresistive properties, the sensors with 0.29 vol% of CNFs were chosen to test piezoresistivity under different loading rates (0.2–5 mm/min).

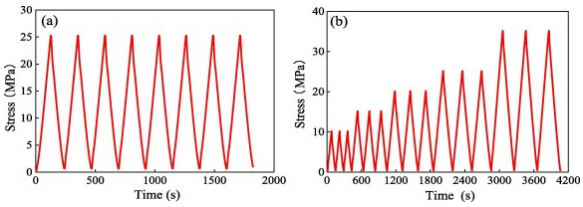

Fig. 2. Cyclic loading paths: (a) loading type 1; (b) loading type 2.

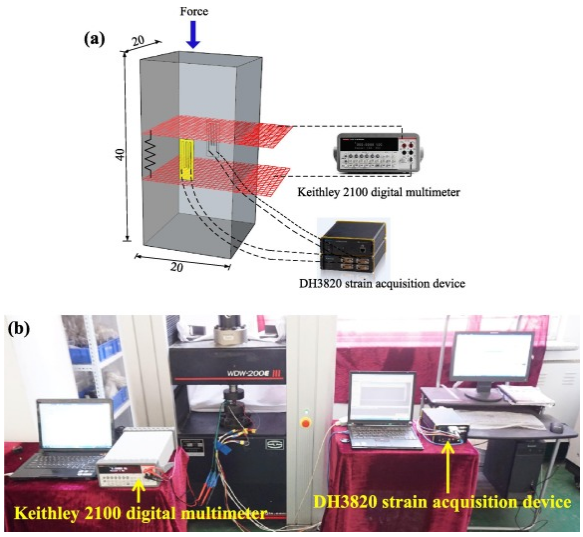

Fig. 3. The experimental setup for piezoresistive test: (a) schematic diagram (units: mm); (b) actual picture.

Because the deformation of the sensors under compression is small, the changes in the separation (L) between the two electrodes can be neglected [34]. Therefore, the fractional change in electrical resistivity (FCR), f, is equivalent to the fractional change in electrical resistance:

$$(1)\ f = \frac{\Delta\rho}{\rho_0} = \frac{\Delta R \times \frac{A}{L}}{R_0 \times \frac{A}{L}} = \frac{\Delta R}{R_0} = \frac{R_t - R_0}{R_0}$$

where $\Delta\rho$ and ΔR are the changes in electrical resistivity and resistance, respectively; ρ_0 and R_0 are the initial resistivity and resistance, respectively, of the sensor without loading; A is the cross-sectional area of the sensor; L is the separation between the two electrodes; and R_t is the resistance at time t during the test.

2.3.2. Temperature effect tests for sensors

Temperature has a significant influence on the CNFs/epoxy sensor, so the effect of temperature on electrical resistivity was investigated. Three specimens for each type of CNFs/epoxy sensor were tested for this purpose. Before temperature variation tests, the specimens were all heated to 60 °C and isothermal treated for 5 min, and then cooled to 20 °C to eliminate the effect of thermal history developed during the preparation process. The sensors were placed in the high-low temperature tester (Lin Pin Co., Ltd., China), and the temperature range was set from −30 to 60 °C at a heating rate of 2 °C/min. The thermosensitive properties of the sensors were measured using the two-electrode method by using the Keithley 2100 digital multimeter in the process of temperature changes. Meanwhile, the strain was monitored by the DH3820 strain acquisition device. In order to investigate the reproducibility of the thermosensitive behaviors, the electric resistivity measurements were conducted for three heating-cooling cycles.

2.3.3. Strain monitoring tests for concrete cylinders

CNFs/epoxy strain sensors were calibrated before they were embedded into concrete cylinders. Concrete cylinders with embedded sensors were subjected to uniaxial compressive load using a hydraulic servo pressure testing machine with 3000 kN capacity. Four displacement transducers were used to measure the local axial deformation of the cylinders. For comparison purposes, three pairs of electrical resistance strain gauges in axial and lateral directions were also glued symmetrically at the opposite sides of the middle section of the cylinders (shown in Fig. 4) to monitor the strains. The corresponding electrical resistance of the embedded CNFs/epoxy sensor was measured simultaneously using the Keithley 2100 digital multimeter. The experimental setup of the strain monitoring test is shown in Fig. 5. In this study, eight concrete cylinders embedded with CNFs/epoxy

sensor were made, in which four cylinders embedded with $S_{0.29}$ and the other four cylinders embedded with $S_{0.58}$. For each type of sensor, two corresponding cylinders were tested under monotonic compressive loads until their failures, and the remaining two cylinders were first subjected to constant cyclic loading and then subjected to incremental amplitude cyclic loading to simulate realistic loading conditions. Responses of the sensors when the cylinders subjected to cyclic loadings were also used to verify the stability and repeatability of the embedded sensors. For the constant amplitude cyclic loading, the peak value was 15 MPa and the valley value was 0.75 MPa. The incremental amplitude cyclic loading was achieved by gradually increasing the loading amplitude to 10, 15, 20, 25 and 35 MPa, respectively. The two loading paths are similar to those of piezoresistive measurement (shown in Fig. 2).

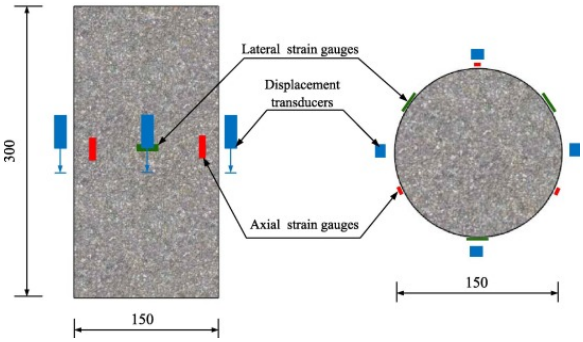

Fig. 4. Layout of strain gauges and displacement transducers (unit: mm).

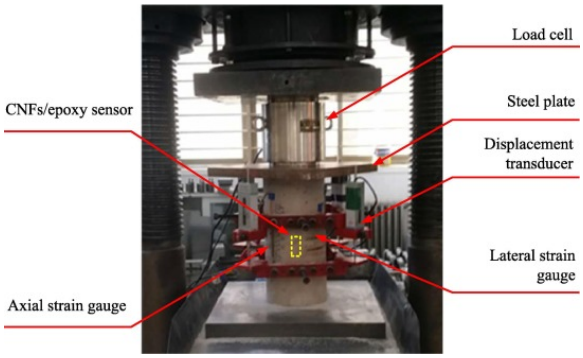

Fig. 5. Experimental setup of strain monitoring test.

3. Results and discussions

3.1. Piezoresistive performances of CNFs/epoxy sensors

3.1.1. Effect of loading rate on piezoresistive performances

The effect of loading rate on piezoresistive performances of CNFs/epoxy sensors was explored to select the appropriate loading rate. Fig. 6 shows FCR vs strain under different loading rates. It shows that the piezoresistive performances of the sensors were almost unaffected by the loading rate lower than 0.4 mm/min, while the noticeable fluctuation of the curve was observed in the case of the loading rate of 1.5 mm/min. This phenomenon reveals that large loading rate could deteriorate the stability of the piezoresistive performances. Therefore, the loading rate of 0.4 mm/min was chosen to ensure the sensors possessing stable piezoresistive performances in the following tests.

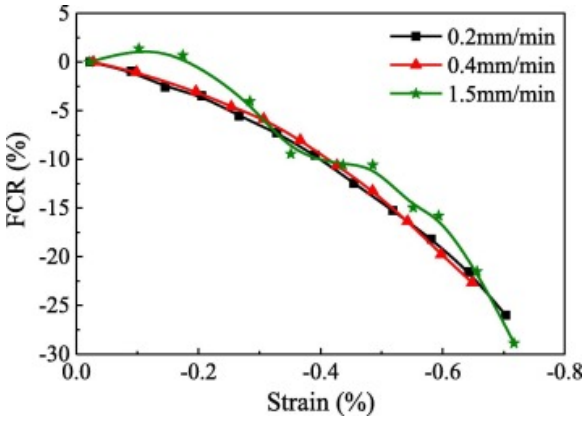

Fig. 6. FCR vs compressive strain under different loading rates.

3.1.2. Piezoresistive performances of CNFs/epoxy sensors under monotonic and cyclic loadings

Fig. 7 shows the variation of FCR under monotonic loading for $S_{0.29}$ and $S_{0.58}$. It can be seen from Fig. 7 that the FCR of the sensors increased linearly with the increase of the applied strain up to a certain value, and then decreased. The piezoresistive behavior is due to the nanoscale structural change in the percolation and corresponds to a stochastic separation of the conducting pathways due to the increased strain. The transition points in Fig. 7 are close to the elastic deformation limits of the sensors, beyond which the specimens enter the plastic zone. The compression of the epoxy matrix leads to a reduction of the distances between the neighboring CNFs. According to the conductive mechanisms, i.e., tunneling conduction theory [35] and percolation conduction (also called contacting conduction) theory [36], a reduction of the distance between CNFs provokes an evident decrease of electrical resistivity. When the specimen enters plastic stage with the increase of load, micro-cracks are initiated and developed in the specimens. Therefore, fewer contacts between the CNFs lead to the decrease of conduction paths. These are believed to be the main reasons that the CNFs/epoxy composites exhibited the piezoresistive responses shown in Fig. 7. For the sensors filled with 0.29 vol% and 0.58 vol% of CNFs, the maximum FCR values are 37% and 50% corresponding to the strains of 1.25% and 1.5%, respectively.

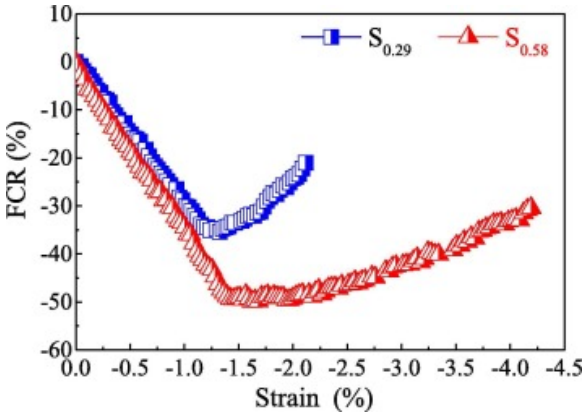

Fig. 7. Response of FCR to strain under monotonic loading.

In order to evaluate the piezoresistive stability of CNFs/epoxy sensors, they were subjected to constant amplitude cyclic loading with a loading rate of 0.4 mm/min firstly. Fig. 8 shows the piezoresistive response of $S_{0.29}$ subjected to constant amplitude cyclic loading. In the subsequent compressing-releasing cycles, the sensor $S_{0.29}$ essentially recovered its resistance after releasing (shown in Fig. 8a). As shown in Fig. 8b, there is a positive

correlation between FCR and strain. $S_{0.58}$ exhibited similar trends as shown in Fig. 9. Therefore, these sensors have clear strain sensitivity with a low noise level.

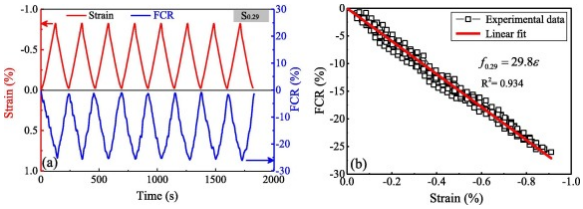

Fig. 8. Piezoresistive performance of $S_{0.29}$ under constant amplitude cyclic loading: (a) FCR and strain vs time; (b) FCR vs strain.

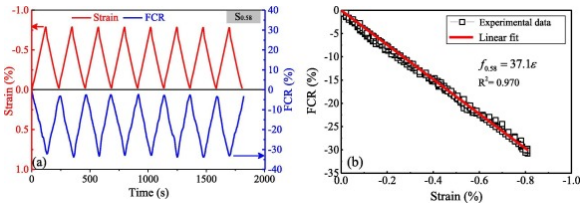

Fig. 9. Piezoresistive performance of $S_{0.58}$ under constant amplitude cyclic loading: (a) FCR and strain vs time; (b) FCR vs strain.

For a more complete understanding of CNFs/epoxy sensors' piezoresistive performances, the relevant parameters including gauge factor, linearity, repeatability and hysteresis were investigated. The relationship between input value ε (compressive strain) and output value f (FCR value) of the sensor was obtained using linear fit by least square method, which can be expressed as

(2) $f_{0.29} = 29.8\varepsilon$

(3) $f_{0.58} = 37.1\varepsilon$

Gauge factor, S, also called strain sensitivity coefficient, which is defined as the ratio between the fractional change in electrical resistance ($\Delta R/R_0$) and the strain (ε), is given by Eq. (4):

(4) $S = \frac{\Delta R/R_0}{\varepsilon}$

Linearity, E, is the offset between strain-FCR curves and the fitted regression line, which is defined as:

(5) $E = \frac{\Delta_{max}}{f_{F,S}} \times 100\%$

where Δ_{max} is the maximum deviation of strain-FCR curves from the fitted regression line, and $f_{F.S}$ is the output range.

Repeatability, R, is the degree of repetition of the output values under same conditions, which is expressed as:

(6) $R = \frac{\Delta R_{max}}{f_{F.S}} \times 100\%$

where ΔR_{max} is the maximum repeat difference, which is the difference of FCR for the same strain in the same process during loading and unloading.

Hysteresis, H, means that the resistivity of the specimens does not completely recover its initial value after unloading in certain cases, which is determined by

(7) $H=\frac{\Delta f_{max}}{f_{F.S}} \times 100\%$

where Δf_{max} is the maximum difference of FCR in all processes during the cyclic loading.

The results of the above parameters are shown in Table 2. It can be observed from Table 2 that $S_{0.58}$ has a better piezoresistive performance compared to $S_{0.29}$. The plot in Fig. 9b also demonstrates good linearity and repeatability of the piezoresistive performances of $S_{0.58}$ by the linear relationship between FCR and strain with very small scatter.

Table 2. Parameters of CNFs/epoxy sensors.

Parameters	Input range (%)	Output range (%)	Gauge factor	Linearity (%)	Repeatability (%)	Hysteresis (%)
$S_{0.29}$	0–0.9	0–26.0	29.8	8.1	6.6	14.6
$S_{0.58}$	0–0.8	0–30.8	37.1	5.5	3.8	6.3

Fig. 10 displays the time histories of strain and FCR for $S_{0.29}$ and $S_{0.58}$ under incremental amplitude cyclic loading. It can be seen that the electrical resistivity of the sensors varied distinctly in response to the applied strain. During each loading cycle, the resistivity values decreased with the increase of compressive strain, resulting in a negative FCR, and then increased to the initial value when the unloading branch of the cycle took place. It can be observed from the figure that the values of FCR increased with the increase of the loading amplitude and the content of CNFs.

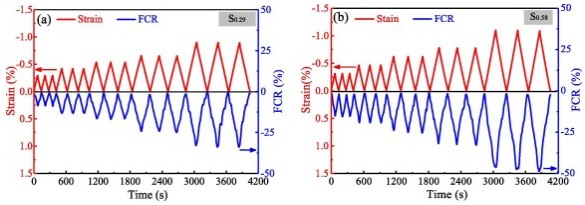

Fig. 10. Time histories of strain and FCR for (a) $S_{0.29}$ and (b) $S_{0.58}$.

3.2. Effect of temperature on electrical resistivity of CNFs/epoxy sensors

Temperature cycling test consisting of three heating-cooling cycles with the range of −30 °C to 60 °C was performed in this section. The reference resistances for this experiment are those at −30 °C. The responses of strain and FCR to temperature for $S_{0.29}$ and $S_{0.58}$ are shown in Fig. 11. There is a clear increase of FCR magnitudes with the temperature growth, and $S_{0.58}$ shows a higher sensitivity towards temperature than that of $S_{0.29}$. It can be observed from Fig. 11a and c that FCR and strain have a similar trend corresponding to the change of temperature, which indicates that the effect of temperature on resistivity is closely related to that of sensors' deformation. The change in dimensions of the CNFs subjected to temperature change is quite small compared to that of the epoxy, and can be ignored. Therefore, when the epoxy expands with the increase of temperature, it increases the distance between CNFs. The increased distance between CNFs increases the tunneling gap, which causes the decrease of the resistivity of the CNFs/epoxy sensors. The plots in Fig. 11b and d demonstrate a high temperature dependence of the CNFs/epoxy sensors, while a slight hysteresis was observed in both $S_{0.29}$ and $S_{0.58}$. The reason for the hysteresis could be the slow volume expansion/contraction processes of the epoxy causing that the internal conductive network could not be restored in time.

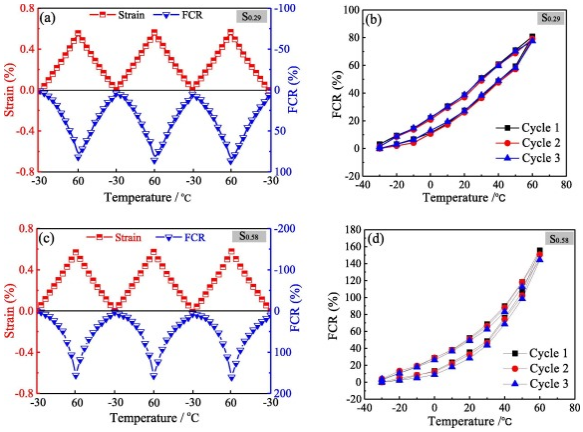

Fig. 11. Responses of strain and FCR to temperature: (a) FCR and strain vs temperature for $S_{0.29}$; (b) FCR vs temperature for $S_{0.29}$; (c) FCR and strain vs temperature for $S_{0.58}$; and (d) FCR vs temperature for $S_{0.58}$.

Temperature compensation is necessary due to the high temperature dependence of the CNFs/epoxy sensors. One of the effective ways to eliminate the influence of temperature on FCR of the sensor is to set up a compensation circuit. The mechanism of the compensation circuit is shown in Fig. 12. In the figure, R_T represents the test sensor and R_C represents the compensation sensor, which is not subjected to the compressive loading. R_1 and R_2 are precision resistors used to balance the bridge voltage. The compensation circuit is similar to the Wheatstone half-bridge configuration. The conditions for effective temperature compensation with a Wheatstone bridge are that all elements have same temperature coefficient and nominal resistance values. According to the compensation circuit, the output value f_T of the test sensor R_T is expressed as:

(8) $f_T = f_T^L + f_T^T + f_T^O$

where f_T^L, f_T^T, and f_T^O are the FCR changes of the test sensor caused by loading, temperature, and other factors, respectively.

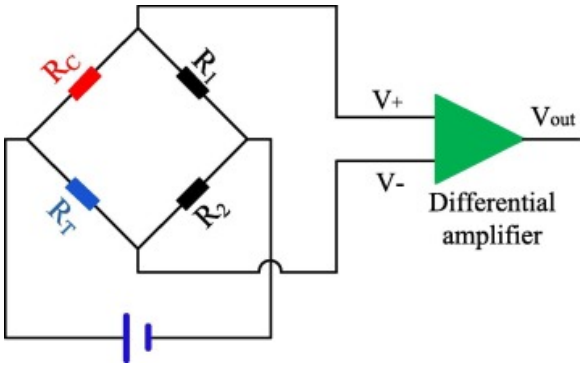

Fig. 12. Schematic of the compensation circuit.

The output value f_C of the compensation sensor R_C is expressed as:

(9) $f_C = f_C^T + f_C^O$

where f_C^T and f_C^O are the FCR changes of the compensation sensor caused by temperature and other factors, respectively.

Based on Eqs. (8), (9), the overall output value f of the compensation circuit is given by:

(10) $f = f_T - f_C = f_T^L + (f_T^T - f_C^T) + (f_T^O - f_C^O)$

Since the test sensor R_T and the compensation sensor R_C have almost exactly same temperature coefficient, nominal resistance values and other performances, the contributions of temperature and other factors to the compensation circuit are negligible, i.e., $f_T^T - f_C^T \approx 0$ and $f_T^O - f_C^O \approx 0$. Therefore, the temperature influence is compensated by the compensation circuit, and the output value of the compensation circuit is

(11) $f = f_T^L$

In order to verify the validity of the compensation circuit, both the test and compensation sensors for $S_{0.29}$ and $S_{0.58}$ were placed in the environment with same temperature, and the output values of the compensation circuit were tested as the temperature was changed. Fig. 13 depicts the output values of $S_{0.29}$ and $S_{0.58}$ with temperature compensation when the environmental temperature was changed from −30 °C to 60 °C. The column charts show the average values with error bars obtained from three samples for each type of sensor. In the entire temperature range from −30 °C to 60 °C, the output value of the compensation circuit was below 1%, which is neglectable compared to that of one sensor without compensation (shown in Fig. 11b and d). It can be observed from Fig. 13 that the compensation circuit can be used to eliminate the influence of temperature on the output value of CNFs/epoxy sensor. In fact, the compensation circuit can be used not only for excluding temperature effect, but also for removing the effect of humidity and other environmental factors. However, the specific effect of humidity on the CNFs/epoxy sensor will be explored in the future study.

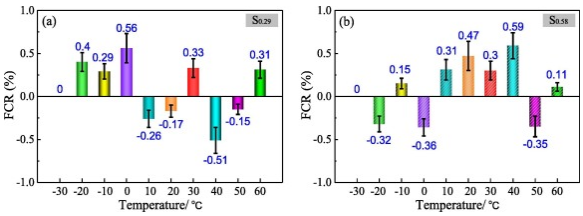

Fig. 13. Output values of (a) $S_{0.29}$ and (b) $S_{0.58}$ with temperature compensation.

Since the volume of the concrete member is not large, the temperature inside and outside of the concrete member is close after the hydration reaction of the concrete is completed. In this case, during the strain monitoring test of concrete cylinder, the temperatures of the test sensors (embedded in concrete cylinder) and the compensation sensors are almost the same. Therefore, the compensation circuit is also suit for the sensors embedded in concrete components.

3.3. Strain monitoring of concrete cylinders with embedded sensors

The previous discussions indicate that CNFs/epoxy sensors have excellent piezoresistive performances. Therefore, they were embedded in concrete cylinders to test their ability to monitor strains in the cylinders subjected to compression. It should be noted that during the initial period of cyclic loading, the peak value of FCR after each cycle showed a downward drift tendency, i.e., the conduction path was unstable. Therefore, pre-pressure for the sensors were carried out in order to achieve a stable conductive state. The calibration of the sensors was also performed before they were embedded into concrete cylinders. The applied strain amplitude during the calibration was about 0.5%, which is in the elastic range of the sensor and would not undermine the monitoring capability of the sensor. Fig. 14 shows typical calibration curves of the two types of sensors under monotonic and cyclic loadings. Based on the calibration curves, the relationship between the strain and FCR value of the sensors during calibration were obtained using linear fit by least square method, which can be expressed as

(12) $\varepsilon_{CS0.29} = 0.032 f_C$
$\varepsilon_{CS0.58} = 0.026 f_C$

where $\varepsilon_{CS0.29}$ and $\varepsilon_{CS0.58}$ are the strains of $S_{0.29}$ and $S_{0.58}$ during calibration, respectively; f_C is the fractional change in resistivity of the sensors during calibration. According to Eq. (12), the gauge factors (the ratio between FCR and strain) of $S_{0.29}$ and $S_{0.58}$ are 31.3 and 38.5, respectively, during calibration.

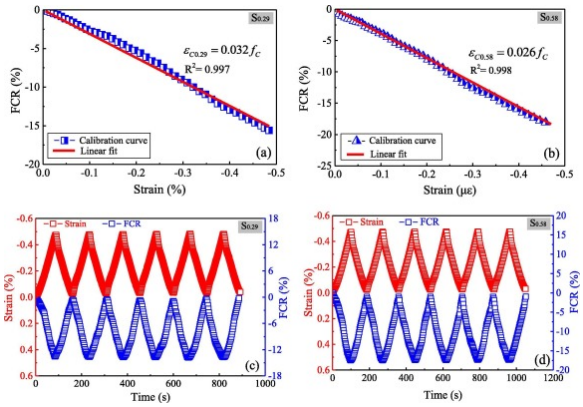

Fig. 14. The calibration curves of two types of sensors: (a) $S_{0.29}$ and (b) $S_{0.58}$ under monotonic loading; (c) $S_{0.29}$ and (d) $S_{0.58}$ under cyclic loading.

The concrete cylinders with embedded sensors were subjected to monotonic compressive loading till their failure and the typical monitoring curves are shown in Fig. 15. The average strength of the concrete cylinders without embedded sensor was 33.5 MPa. The average strengths of the concrete cylinders embedded with $S_{0.29}$ and $S_{0.58}$ were 32.6 MPa and 32.1 MPa, respectively. Because the size of the sensor is much smaller than that of the concrete structural members, the sensor has little effect on the strength of the concrete members. In addition, the study of Xiao et al. [30] shows that the strengths of concrete columns with embedded sensors were only slightly lower than those of concrete columns without embedded sensors, which indicates that the effect of sensors embedment on mechanical property is small and can be negligible. It can be observed from Fig. 15 that the FCR of the sensors increased linearly with the increase of the applied strain. Based on the monitoring curves, the relationships between the strains of the cylinder and the FCR values of the sensors during monitoring were obtained using linear fit by least square method, which can be expressed as

$$(13)\quad \begin{matrix} \varepsilon_{MS0.29} = 0.013 f_M \\ \varepsilon_{MS0.58} = 0.012 f_M \end{matrix}$$

where $\varepsilon_{MS0.29}$ and $\varepsilon_{MS0.58}$ are the strains of concrete cylinders embedded with $S_{0.29}$ and $S_{0.58}$ during monitoring, respectively; f_M is the fractional change in resistivity of the sensors during monitoring. Similarly, according to Eq. (13), the gauge factors of $S_{0.29}$ and $S_{0.58}$ are 76.9 and 83.3 during monitoring, respectively. In addition, the strength of the embedded sensors should match with that of concrete structures to avoid failing earlier than the monitoring object. The compressive strength of the CNFs/epoxy sensor was about 75 MPa, which is larger than two times of that of the concrete cylinders (33.5 MPa). Moreover, it was observed that the CNFs/epoxy sensors in the broken concrete cylinders were intact after the axial compression test, which indicates that the sensor is able to monitor the whole damage process of the concrete component.

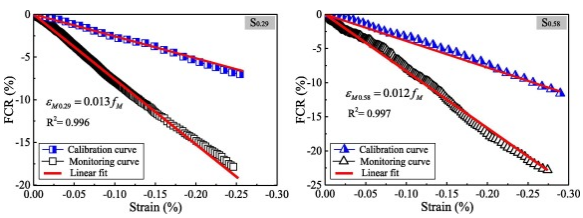

Fig. 15. The monitoring and calibration curves of two types of sensors under monotonic loading.

Fig. 15 also presents a comparison between the calibration and monitoring curves of the sensors. It can be observed from Fig. 15 that there is a mismatch between the calibration and monitoring curves. The Poisson's ratio of CNF/epoxy sensor (about 0.4) is about twice as much as that of the concrete cylinder (approximately 0.2), and the elastic modulus of the sensor (3.2 GPa) is much smaller than that of the concrete cylinder (28.9 GPa). Because of the differences of the elastic moduli and the Poisson's ratios between the concrete cylinders and the CNFs/epoxy sensors, the sensors' lateral deformations were confined by the surrounding concrete. Based on the conductive mechanism of the composite, the lateral deformation of the sensor is reduced, leading to a decrease in the spacing of the internal CNFs. This is conducive to the formation of conductive paths. Therefore, the FCR of the lateral constrained sensor is larger when the same axial strain is applied. According to the definition of the gauge factor (S) shown in Eq. (4), the sensors embedded in concrete cylinders subjected to axial compression had larger gauge factors than the sensors themselves during calibration. This is the reason why a mismatch between the two types of curves happened as shown in Fig. 15. An effective way to solve this mismatch problem is to introduce a correction factor, k, so that the strain of the concrete cylinders measured by the CNFs/epoxy sensor is consistent with that measured by the traditional electrical resistance strain gauge. The strains measured by CNFs/epoxy sensors can be obtained by dividing the FRC values by the gauge factors of the sensors. By comparing Eqs. (12) and (13), the correction factors for $S_{0.29}$ and $S_{0.58}$ are 0.41 and 0.46, respectively. The correction factor is closely related to the performance of sensors and concrete components. Therefore, the correction factor here is only valid for the concrete used in this study. The correct factor should be tested and calibrated when the sensor is used for different concrete. The relationships of strain values between calibration and monitoring can be expressed as

$$(14)\quad \begin{matrix} \varepsilon_{MS0.29} = 0.41\varepsilon_{CS0.29} \\ \varepsilon_{MS0.58} = 0.46\varepsilon_{CS0.58} \end{matrix}$$

In order to simulate real loading conditions and verify the stability and repeatability of the embedded sensors, constant and incremental amplitude cyclic loadings were applied to the cylinders. The maximum stress for monitoring test was 15 MPa, which was same as the amplitude of the applied stress during calibration. The typical monitoring curves of two types of sensors under constant and incremental amplitude cyclic loadings are shown in Fig. 16. These curves depict the relationship between the FCR of sensors and the strain of the cylinders. However, a little fluctuation of the monitoring curves was observed as the cylinders and sensors were subjected to cyclic loadings. Fig. 16 shows that the instantaneous response of the FCR closely follows the change of the strain, which indicates that the resistivity of the sensor varies synchronously with the strain of the cylinder. Fig. 17 shows the strains of concrete cylinders under constant and incremental amplitude cyclic loadings, measured by CNFs/epoxy sensors and traditional resistance strain gauges, respectively. Strain measured by CNFs/epoxy sensors was obtained by dividing the FRC values with the gauge factors of $S_{0.29}$ and $S_{0.58}$ (76.9 and 83.3, respectively). As shown in Fig. 17, the strains measured by CNFs/epoxy sensors agree well with those of electrical resistance strain gauges. However, the electrical resistance strain gauges were glued at the surface of the cylinders and the CNFs/epoxy sensors were embedded inside the cylinders. In addition, the test lengths of the electrical resistance strain gauges are longer than that of CNFs/epoxy sensors. Therefore, the slight difference between the two monitoring results may be derived from the difference in the measuring range and the location of the two monitoring devices. The experimental results reveal that the repeatability and stability of strain monitoring of embedded CNFs/epoxy sensors are reliable. However, it is not sensitive to the damage of the concrete cylinder. Therefore, when the concrete specimens have micro or meso cracks, the performance of the sensor should not change significantly, which is in agreement with the studies of Ou and Han [29], and Xiao et al. [30].

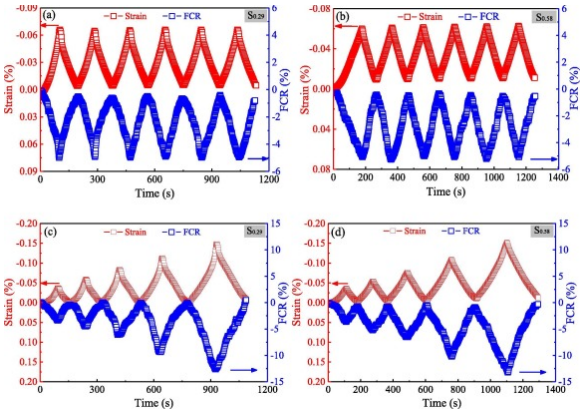

Fig. 16. The monitoring curves of two types of sensors: (a) $S_{0.29}$ and (b) $S_{0.58}$ under constant amplitude cyclic loading; (c) $S_{0.29}$ and (d) $S_{0.58}$ under incremental amplitude cyclic loading.

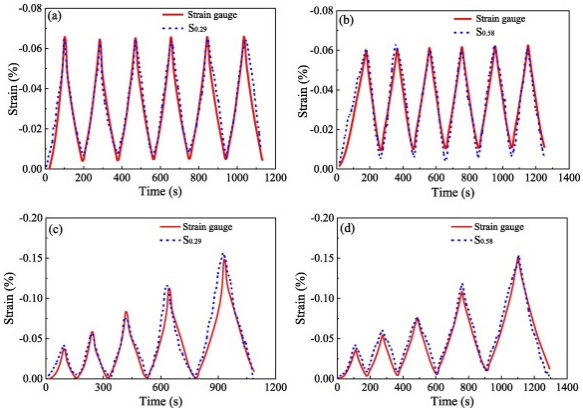

Fig. 17. Strains of concrete cylinders measured by electrical resistance strain gauge and CNFs/epoxy sensors under different types of loadings: (a) $S_{0.29}$ and (b) $S_{0.58}$ under constant amplitude cyclic loading; (c) $S_{0.29}$ and (d) $S_{0.58}$ under incremental amplitude cyclic loading.

4. Conclusions

The embedded strain sensors based on the principle of piezoresistivity were fabricated by epoxy-based composites filled with two contents of CNFs. CNFs/epoxy sensors were embedded in concrete cylinders to monitor their strains under monotonic and cyclic loadings. Both types of embedded CNFs/epoxy sensors exhibited excellent piezoresistive performances and strain-monitoring capability. The following conclusions can be drawn from this study:

1) The sensor filled with 0.58 vol% of CNFs possesses better piezoresistive performance compared to that with 0.29 vol% of CNFs.
2) Temperature compensation is necessary due to the high temperature dependence of the CNFs/epoxy sensors. The proposed compensation circuit with a half bridge configuration can eliminate the influence of temperature on sensing signals of the sensors.
3) The strains measured by the embedded CNFs/epoxy sensors agree well with those of electrical resistance strain gauges after modifying the gauge factors of the sensors, which reveals that the embedded CNFs/epoxy sensors can be used to monitor the compressive strain of concrete components.

Conflict of interest

None.

Acknowledgments

This work was supported by the National Key R&D Program of China (Project No. 2017YFC0703008), the National Natural Science Foundation of China (Project No. 51778102), the Fundamental Research Funds for the Central Universities (Project No. DUT18LK35) and the State Scholarship Fund of China (Project No. 201706060249).

References

[1] F. Azhari, N. Banthia **Cement-based sensors with carbon fibers and carbon nanotubes for piezoresistive sensing** *Cem. Concr. Compos.*, 34 (2012), pp. 866-873

[2] F. Naeem, H.K. Lee, H.K. Kim, I.W. Nam **Flexural stress and crack sensing capabilities of MWNT/cement composites** *Compos. Struct.*, 175 (2017), pp. 86-100

[3] P. Ferreira, E. Caetano, L. Ramos, P. Pinto **Shape sensing monitoring system based on fiber-optic strain measurements: laboratory tests** *Exp. Tech.*, 41 (2017), pp. 407-420

[4] X. Ma, G. Wei **Numerical prediction of effective electro-elastic properties of three-dimensional braided piezoelectric ceramic composites** *Compos. Struct.*, 180 (2017), pp. 420-428

[5] D. Chung **Self-heating structural materials** *Smart Mater. Struct.*, 13 (2004), pp. 562-565

[6] B. Han, Y. Wang, S. Dong, L. Zhang, S. Ding, X. Yu, *et al.* **Smart concretes and structures: a review** *Intell. Mater. Syst. Struct.*, 26 (2015), pp. 1303-1345

[7] E. García-Macías, A. D'Alessandro, R. Castro-Triguero, D. Pérez-Mira, F. Ubertini **Micromechanics modeling of the uniaxial strain-sensing property of carbon nanotube cement-matrix composites for SHM applications** *Compos. Struct.*, 163 (2017), pp. 195-215

[8] B.F. Gonçalves, J. Oliveira, P. Costa, V. Correia, P. Martins, G. Botelho, S. Lanceros-Mendez **Development of water-based printable piezoresistive sensors for large strain applications** *Compos. Part B Eng.*, 112 (2017), pp. 344-352

[9] J.T. Shen, S.T. Buschhorn, J.T.M. De Hosson, K. Schulte, B. Fiedler **Pressure and temperature induced electrical resistance change in nano-carbon/epoxy composites** *Compos. Sci. Technol.*, 115 (2015), pp. 1-8

[10] R.B. Ladani, S. Wu, A.J. Kinloch, K. Ghorbani, J. Zhang, A.P. Mouritz, C.H. Wang **Improving the toughness and electrical conductivity of epoxy nanocomposites by using aligned carbon nanofibers** *Compos. Sci. Technol.*, 117 (2015), pp. 146-158

[11] Y. Wang, Y. Wang, B. Wan, B. Han, G. Cai, Z. Li **Properties and mechanisms of self-sensing carbon nanofibers/epoxy composites for structural health monitoring** *Compos. Struct.*, 200 (2018), pp. 669-678

[12] R.B. Ladani, S. Wu, A.J. Kinloch, K. Ghorbani, J. Zhang, A.P. Mouritz, C.H. Wang **Multifunctional properties of epoxy nanocomposites reinforced by aligned nanoscale carbon** *Mater. Des.*, 94 (2016), pp. 554-564

[13] Y. Wang, R. Chang, G. Chen **Strain and damage self-sensing properties of carbon nanofibers/carbon fiber-reinforced polymer laminates** *Adv. Mech. Eng.*, 9 (2017), pp. 1-11

[14] R. Moriche, M. Sánchez, A. Jiménez-Suárez, S.G. Prolongo, A. Ureña **Strain monitoring mechanisms of sensors based on the addition of graphene nanoplatelets into an epoxy matrix** *Compos. Sci. Technol.*, 123 (2016), pp. 65-70

[15] H.P.S. Abdul Khalil, M. Jawaid, P. Firoozian, M. Amjad, E. Zainudin, M.T. Paridah **Tensile electrical conductivity, and morphological properties of carbon black-filled epoxy composites** *Int. J. Polym. Anal. Charact.*, 18 (2013), pp. 329-338

[16] B.G. Han, B.Z. Han, J.P. Ou **Experimental study on use of nickel powder-filled Portland cement-based composite for fabrication of piezoresistive sensors with high sensitivity** *Sens. Actuators, A,* 149 (2009), pp. 51-55

[17] H. Aguilar-Bolados, M.A. Lopez-Manchado, J. Brasero, F. Avilés, M. Yazdani-Pedram **Effect of the morphology of thermally reduced graphite oxide on the mechanical and electrical properties of natural rubber nanocomposites** *Compos. Part B Eng*., 87 (2016), pp. 350-356

[18] X. Wei, X. Cao, Y. Wang, G. Zheng, K. Dai, C. Liu, C. Shen **Conductive herringbone structure carbon nanotube/thermoplastic polyurethane porous foam tuned by epoxy for high performance flexible piezoresistive sensor** *Compos. Sci. Technol*., 149 (2017), pp. 166-177

[19] B. Han, L. Zhang, C. Zhang, Y. Wang, X. Yu, J. Ou **Reinforcement effect and mechanism of carbon fibers to mechanical and electrically conductive properties of cement-based materials** *Constr. Build. Mater*., 125 (2016), pp. 479-489

[20] W. Li, X. Li, S.J. Chen, Y.M. Liu, W.H. Duan, S.P. Shah **Effects of graphene oxide on early-age hydration and electrical resistivity of Portland cement paste** *Constr. Build. Mater*., 136 (2017), pp. 506-514

[21] W. Li, M. Asce, X. Li, S.J. Chen, G. Long **Effects of nanoalumina and graphene oxide on early-age hydration and mechanical properties of cement paste** *J. Mater. Civ. Eng*., 29 (2017), pp. 1-9

[22] Q. Liu, R. Gao, V.W.Y. Tam, W. Li, J. Xiao **Strain monitoring for a bending concrete beam by using piezoresistive cement-based sensors** *Constr. Build. Mater*., 167 (2018), pp. 338-347

[23] Y. Wang, G. Chen, B. Wan, H. Lin, J. Zhang **Behavior of innovative circular ice filled steel tubular stub columns under axial compression** *Constr. Build. Mater*., 171 (2018), pp. 680-689

[24] R. Liu, H. Xiao, H. Li, L. Sun, Z. Pi, G.Q. Waqar, T. Du, L. Yu **Effects of nano-SiO_2 on the permeability-related properties of cement-based composites with different water/cement ratios** *J. Mater. Sci.,* 53 (2018), pp. 4974-4986

[25] J. Luo, K.L. Chung, Q. Li, S. Chen, L. Li, D. Hou, C. Zhang **Piezoresistive properties of cement composites reinforced by functionalized carbon nanotubes using photo-assisted Fenton** *Smart Mater. Struct*., 26 (2017), p. 35025

[26] H. Xiao, M. Liu, G. Wang **Anisotropic electrical and abrasion-sensing properties of cement-based composites containing aligned nickel powder** *Cem. Concr. Compos*., 87 (2018), pp. 130-136

[27] A.O. Monteiro, A. Loredo, P.M.F.J. Costa, M. Oeser, P.B. Cachim **A pressure-sensitive carbon black cement composite for traffic monitoring** *Constr. Build. Mater*., 154 (2017), pp. 1079-1086

[28] I.W. Nam, S.M. Park, H.K. Lee, L. Zheng **Mechanical properties and piezoresistive sensing capabilities of FRP composites incorporating CNT fibers** *Compos. Struct*., 178 (2017), pp. 1-8

[29] J. Ou, B. Han **Piezoresistive cement-based strain sensors and self-sensing concrete components** *J. Intell. Mater. Syst. Struct.,* 20 (2009), pp. 329-336

[30] H. Xiao, H. Li, J. Ou **Self-monitoring properties of concrete cylinders with embedded cement-based strain sensors** *J. Intell. Mater. Syst. Struct.,* 22 (2011), pp. 191-200

[31] H. Xiao, H. Li, J. Ou **Strain sensing properties of cement-based sensors embedded at various stress zones in a bending concrete beam** *Sens. Actuators, A,* 167 (2011), pp. 581-587

[32] A. D'Alessandro, F. Ubertini, E. García-Macías, R. Castro-Triguero, A. Downey, S. Laflamme, A. Meoni, A.L. Materazzi **Static and dynamic strain monitoring of reinforced concrete components through embedded carbon nanotube cement-based sensors** *Shock Vib*., 2017 (2017)

[33] L. Zhang, S. Ding, S. Dong, Z. Li, J. Ouyang, X. Yu, B. Han **Piezoresistivity, mechanisms and model of cement-based materials with CNT/NCB composite fillers** *Mater. Res. Express*, 4 (2017), Article 125704

[34] X. Xu **Intelligent Pavement for Traffic Flow Detection-Phase II** University of Minnesota Duluth, Minneapolis (2012), p. 19

[35] W. Wang, T. Lee, M.A. Reed **Mechanism of electron conduction in self-assembled alkanethiol monolayer devices** Ann. N. Y. Acad. Sci., 1006 (2003), pp. 21-35

[36] L. He, S.C. Tjong **Low percolation threshold of graphene/polymer composites prepared by solvothermal reduction of graphene oxide in the polymer solution** *Nanoscale Res. Lett*., 8 (2013), pp. 2-8